PITHA 02/19
LC-DET-2002-022
physics/0212005

Modelling and Measurement of Charge Transfer in Multiple GEM Structures

M. Killenberg, S. Lotze, J. Mnich, S. Roth *, R. Schulte, B. Sobloher, W. Struczinski †, M. Tonutti

III. Physikalisches Institut, RWTH Aachen, D-52056 Aachen, Germany

Abstract

Measurements and numerical simulations on the charge transfer in Gas Electron Multiplier (GEM) foils are presented and their implications for the usage of GEM foils in Time Projection Chambers are discussed. A small test chamber has been constructed and operated with up to three GEM foils. The charge transfer parameters derived from the electrical currents monitored during the irradiation with an ^{55}Fe source are compared with numerical simulations. The performance in magnetic fields up to 2 T is also investigated.

Key words: Time Projection Chamber, TPC; Gas Electron Multiplier, GEM;
PACS: 29.40.Cs, 29.40.Gx

1 Introduction

A Time Projection Chamber (TPC) is foreseen as the main tracker of the detector for the TESLA linear collider [1]. It should provide a momentum resolution of $\delta(1/p_t) < 2 \cdot 10^{-4}(\mathrm{GeV/c})^{-1}$ to exploit especially the physics of final states with high energy leptons. In addition, the specific ionisation

* Corresponding author. *Phone:* +49–241–80–27298; *Fax:* +49–241–80–22244; *Email:* roth@physik.rwth-aachen.de

† Deceased.

dE/dx will be measured with a precision better than 5% to allow particle identification in hadronic jets.

To reach these goals readout planes with the finest possible granularity are required. They must provide a single point resolution of 100 – 150 μm and their systematic distortions must be controlled to better than 10 μm over the whole radius of 1.6 m. Enough charge amplification has to be provided by the system to keep the signals well above the noise level of modern readout electronics. At the same time the produced ions have to be suppressed intrinsically, because active gating is not possible in between a TESLA bunch spacing of 337 ns and is only feasible in between bunch trains. Finally one aims for a minimum of material in front of the calorimeters, especially in the endcap region.

A conventional TPC using a multi wire plane for charge amplification has limitations due to the $\vec{E} \times \vec{B}$ effects in the region close to the wires. In strong magnetic fields these effects depend on the projected angle between the track and the wire and in general result in a broadening of the electron cloud and a worsening of the resolution. In addition, as the wires define a preferred direction, the reconstructed hit location depends on this projected track-wire angle. The readout is done via pads which detect the induced signals from the wires. This induced signal is broader than the cloud of arriving electrons and limits the granularity of the TPC as well as the double track resolution.

Using Gas Electron Multipliers (GEM) [2] as the charge amplifying system could solve some of the drawbacks of wire planes. A GEM consists of a polymer foil about 50 μm thick and metal coated on both sides. It is perforated by a high density of small holes with diameters of typically 50 – 100 μm. Voltages up to 500 V between the two conducting sides generate high electric fields of order 80 kV/cm inside the holes where the gas amplification of the drifting electrons occurs. When using GEM structures for the TPC end plate, the pads directly detect the amplified electron cloud which results in a fast and narrow charge signal. Also the slow ion tail is cut off since the ion cloud does not reach the induction region. A GEM foil shows no preferred direction, thus $\vec{E} \times \vec{B}$ effects will be isotropic. And finally, using highly different electric fields in front and behind the GEM, the back drift of ions produced inside the GEM holes (*ion feedback*) can be largely suppressed.

To demonstrate the advantages of a TPC with GEM readout a prototype chamber will be built within the R&D activities of the linear collider TPC group [6]. It will be used to investigate whether the momentum accuracy, the double track resolution and the quality of the dE/dx measurement as demanded for a detector at TESLA can be reached. The end plates of this prototype will contain up to three planes of charge amplifying GEM foils. The operation conditions of this multi GEM structure should be optimised beforehand, because in the case of three GEM planes six electric fields have to be set. For these studies a small test stand was set up at the RWTH Aachen.

The optimisation of a TPC readout plane will involve three important parameters:

- The *electron transparency*, T_{elec}, i.e. the fraction of primary ionisation that experiences multiplication, should be near to 100%.
- The *effective gain*, G_{eff}, i. e. the number of electrons reaching the anode pads per primary electron, should be sufficiently high.
- The *ion feedback*, B_{ion}, i. e. the fraction of ions that reach the cathode plane, should be at a minimum.

To study the charge transfer mechanism of GEM structures we first introduce the following variables for a single GEM foil:

- The *collection efficiency*, $C^{-(+)}$, i.e. the fraction of electrons (ions) collected into the GEM holes per number of electrons (ions) arriving.
- The *gain*, G, i.e. the factor by which the number of electrons is increased by gas multiplication inside the GEM holes
- The *extraction efficiency*, $X^{-(+)}$, i.e. the fraction of electrons (ions) extracted from the GEM holes into the drift volume per number of electrons (ions) produced in the holes.
- The *secondary extraction efficiency*, X^{+}_{sec}, i.e. the fraction of ions extracted from the GEM holes into the drift volume per number of ions which had been collected into the holes. This is different from the primary extraction, X^{+}, as will become clear in Section 4.

These *transfer coefficients* have been determined as a function of the electric and magnetic fields by measuring the various currents that appear on the electrodes of the GEM structure. Numerical simulations of the electric field fluxes allowed us to predict these variables and to compare the prediction with measurements. Additionally a parametrisation of the simulation has been established which can be used in future to optimize the working point of the GEM structure with respect to ion feedback and transparency.

2 The Test Chamber

2.1 Mechanical Setup

The test chamber is built on a PC board which is used as the anode plane. The sensitive area consists of a solid copper electrode of the same size as the GEM structures (10×10 cm^2). A bolt made of non conducting material is

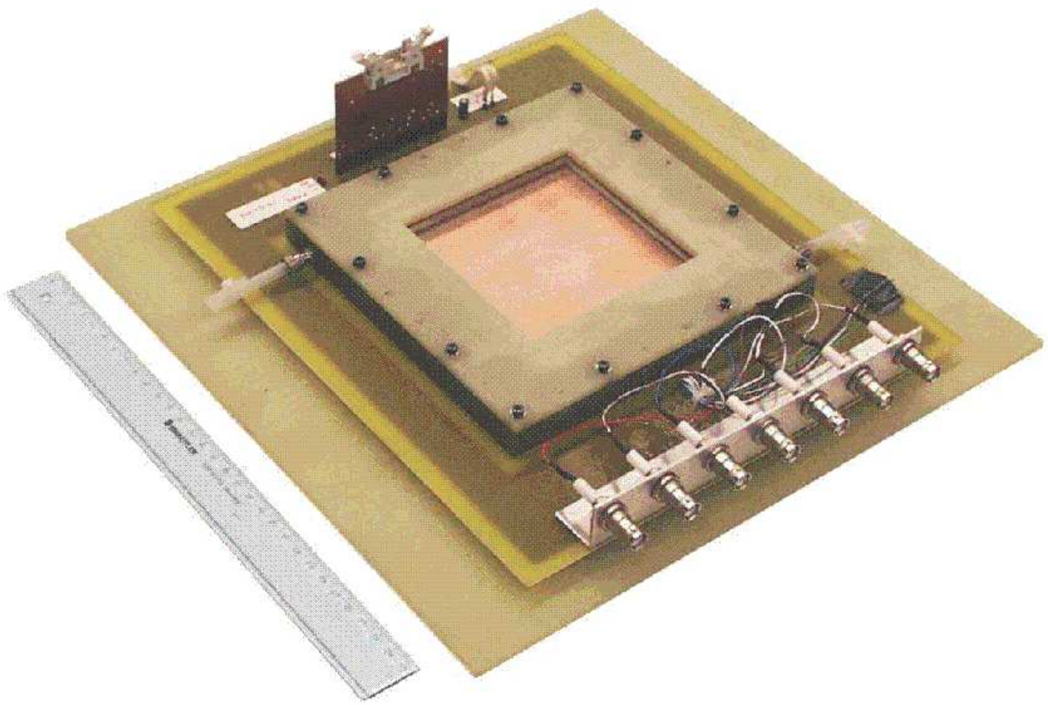

Fig. 1. The test chamber used for the measurements

fixed in each of the four corners This allows the mounting of up to three GEM foils glued on frames with corresponding holes. The distances between the GEM foils (typically 2 mm) can be set by spacers. On top of the last GEM the cathode, consisting of a fine metal mesh, is fixed in the same way as the GEMs. The gas volume is closed on the sides by a composite frame. The top is covered by a 24 μm thick mylar foil which allows the photons from an ^{55}Fe source to penetrate into the chamber.

The chamber has been operated alternatively with Ar/CO_2 82/18 for the measurements without a magnetic field (Section 4) or with Ar/CH_4 95/5 for the magnet tests at a rate of 2-6 l/h (Section 5). It was irradiated from the top by an ^{55}Fe source with an activity of the order of 100 MBq.

2.2 Electric Setup

Each electrode (GEM surfaces and cathode) is connected to an individual channel of a CAEN SY127 HV power supply, allowing the flexible setting of all electric fields and GEM voltages. Nano-Amperemeters [3], constructed in our electronics workshop which provide a resolution of approximately 0.1 nA, are inserted in the supply line of each HV channel. To measure the anode current, all pads and the surrounding copper are connected to ground via an individual nanoamperemeter. The high voltage control and current readout

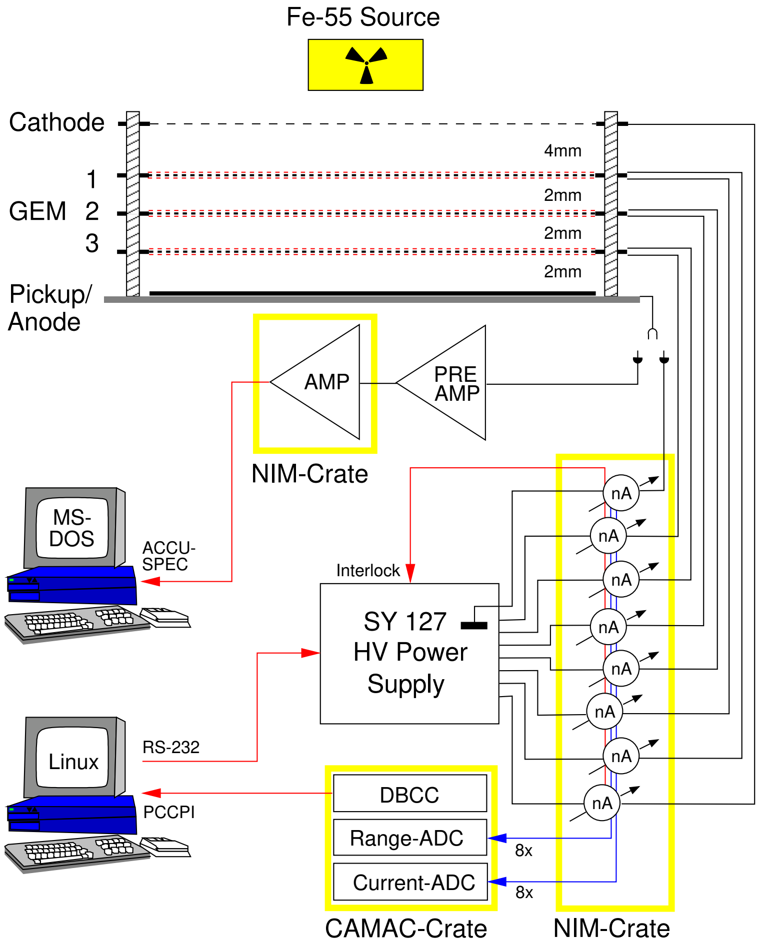

Fig. 2. Experimental setup for the current measurements

are handled by a custom application running on a Linux system.

2.3 Analysis

In Section 1, the charge transfer coefficients are defined as ratios of charges. We use the corresponding currents, as charges are produced and transferred continuously. These currents of drifting electrons and Ions (I_D, $I_{T,n}$, $I_{Hole,n}$ and I_I in Figure 3) cannot be measured directly, but have to be calculated from the currents transferred on the electrodes (I_C, $I_{GEM,n,C/A}$, I_A). The fact that every current has an electron and an ion component must be considered when calculating transfer coefficients for electrons or ions separately. Depending on the individual setup and coefficient, this can become quite complex. Details are described in [4].

As an example, consider the electron extraction efficiency for GEM3. This is defined as the fraction of electrons extracted from the GEM holes into the induction region per number of electrons produced in the holes, and can be

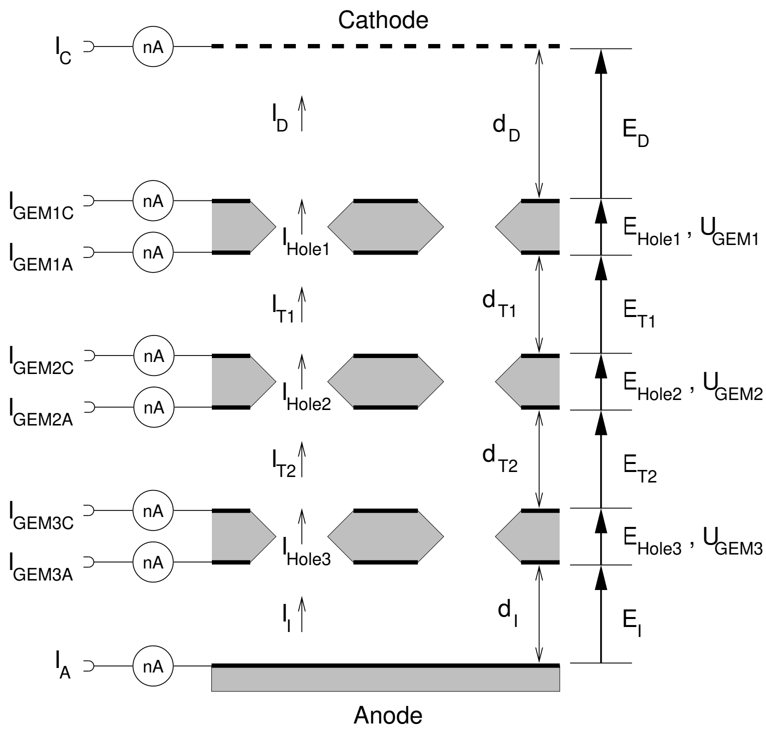

Fig. 3. Assignment of fields and currents to the corresponding electrodes; the volumes surrounding the GEMs are referred to as $\underline{d}$rift, $\underline{t}$ransfer, and $\underline{i}$nduction regions (from top to bottom).

calculated from the measured currents as

$$X^{-} = \frac{I_A}{I_A + I_{GEM3A}} \; .$$

This is a simple case, because in the region below GEM3 only electrons exist.

3 Numerical Simulations and Parametrisations

The numerical simulations are performed using the finite element program Maxwell 3D of Ansoft Co. [9]. It allows the solution of the Maxwell equations in three dimensional problems. For the simulation of the electric fields inside and between the GEM structures only the electrostatic problem solver is needed.

First the geometry of a unit cell of the GEM is constructed with the CAD part of the program. Material properties are assigned to the geometrical objects using the database provided. Above and below the GEM foil 200 μm of material-free drift field are added to the model. Then electric potentials are assigned to each conducting plane. The boundary conditions at the border of the simulated unit cell are chosen such that the electric field is parallel to the

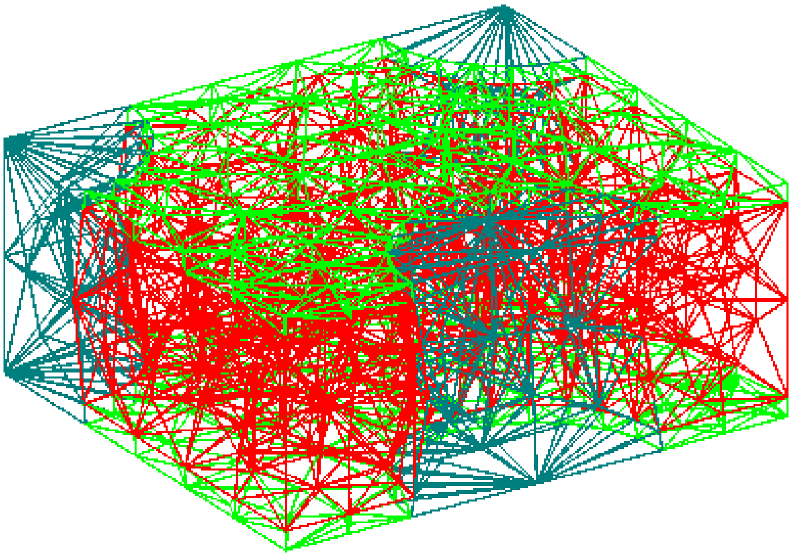

Fig. 4. Coarse finite element mesh generated with Maxwell 3D

border planes (Neumann boundaries).

Maxwell generates the finite element mesh by dividing the model volume into small tetrahedrons. The mesh can be refined in critical regions like sharp edges for example. The electric potential is calculated at each knot and each centre of the connection lines of the mesh by solving the Poisson equation numerically. Inside the tetrahedrons the potential is interpolated by a second order polynomial.

After a numerical solution has been found, it can be visualized using the post processor. For example, field vectors or potential lines can be drawn, but also further calculations can be applied to the solution found. Especially mean electric fields or the electric flux through different areas is used extensively throughout this analysis. For details of the simulation studies, see [5].

3.1 Electric field inside the GEM hole

One of the most important parameters of a GEM structure is the mean electric field inside a GEM hole, E_{hole}. We define this parameter from the integral of the electric field over the area of the hole centre, A ($\vec{n}$ is its normal vector):

$$E_{\mathrm{hole}} = \frac{\int_A \vec{E} \cdot \vec{n} \; d^2r}{\int_A \; d^2r} \tag{1}$$

The calculated field depends on the GEM geometry used, the voltage across the GEM foil and the electric fields of the drift regions above and below the

GEM, as shown in Figure 5. The plot suggests the following linear parametrisation

$$E_{\text{hole}} = a \cdot U_{\text{GEM}} + b \cdot (E_D + E_I)\ , \tag{2}$$

where a and b are parameters depending on the GEM geometry.

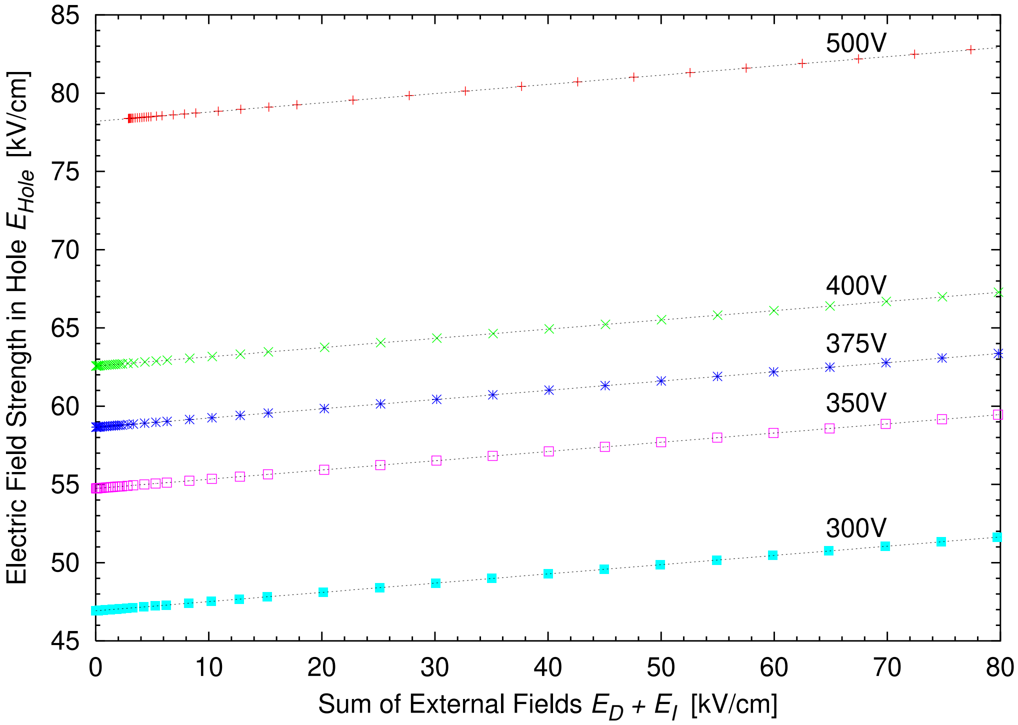

Fig. 5. Electric field strength in GEM hole for several GEM voltages and different external fields

3.2 Electric field flux and charge transfer coefficients

Neglecting diffusion effects across the GEM structure and assuming zero magnetic field, all charges (electrons and ions) will follow the electric field lines. It is also assumed that during gas multiplication charges are spread homogeneously across the complete cross section of the GEM hole. In this model it is possible to calculate the charge transfer coefficients from the electric field flux.

Figure 6 shows a schematic plot of the electric flux through a GEM hole. The total flux coming from the anode Φ_{anode} and the flux going to the cathode Φ_{cathode} can be calculated from a surface integral over the electric field at the bottom and top of the GEM model, respectively. The total flux through the GEM hole is again the flux integral over the area of the hole centre.

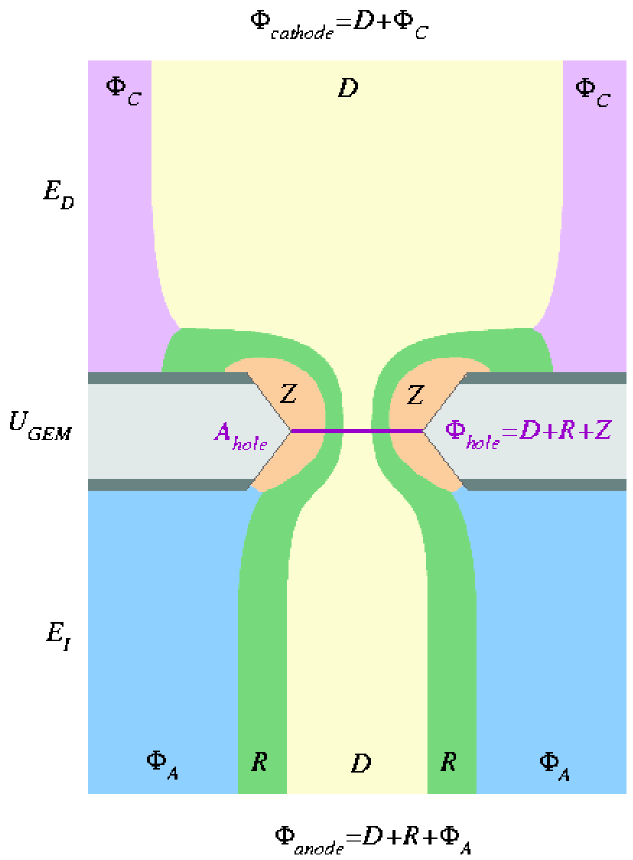

Fig. 6. Model of the electric flux for one GEM hole in an asymmetric field configuration. (Different electric fields above and below the GEM foil.)

Furthermore, the electric flux can be separated into contributions from distinct regions illustrated by different shades in Figure 6. There are the fluxes Φ_{C} and Φ_{A} which go directly from the electrodes to the copper planes of the GEM. The direction of the electric field changes between region Φ_{C} and R and between Φ_{A} and Z. Therefore Φ_{C} and Φ_{A} can be extracted by a numerical integration over that part of the copper plane, where the electric field is pointing upwards. The electric flux D which goes from one electrode through the GEM hole directly to the other electrode, the flux R from the anode through the hole onto the top side of the GEM surface and the flux Z going from the lower to the upper GEM surface cannot be calculated directly.

The collection efficiency C is the fraction of the external flux that is collected into the GEM hole:

$$C_{\mathrm{top}} = \frac{D}{\Phi_{\mathrm{cathode}}} = \frac{\Phi_{\mathrm{cathode}} - \Phi_{\mathrm{C}}}{\Phi_{\mathrm{cathode}}}, \quad C_{\mathrm{bottom}} = \frac{D+R}{\Phi_{\mathrm{anode}}} = \frac{\Phi_{\mathrm{anode}} - \Phi_{\mathrm{A}}}{\Phi_{\mathrm{anode}}} \tag{3}$$

The extraction efficiency X can be calculated from the fraction of the total electric flux originating from the hole and leaving the GEM structure towards cathode or anode:

$$X_{\text{top}} = \frac{D}{\Phi_{\text{hole}}} = \frac{\Phi_{\text{cathode}} - \Phi_{\text{C}}}{\Phi_{\text{hole}}}, \quad X_{\text{bottom}} = \frac{D + R}{\Phi_{\text{hole}}} = \frac{\Phi_{\text{anode}} - \Phi_{\text{A}}}{\Phi_{\text{hole}}} \tag{4}$$

3.3 Simulation results and parametrisation

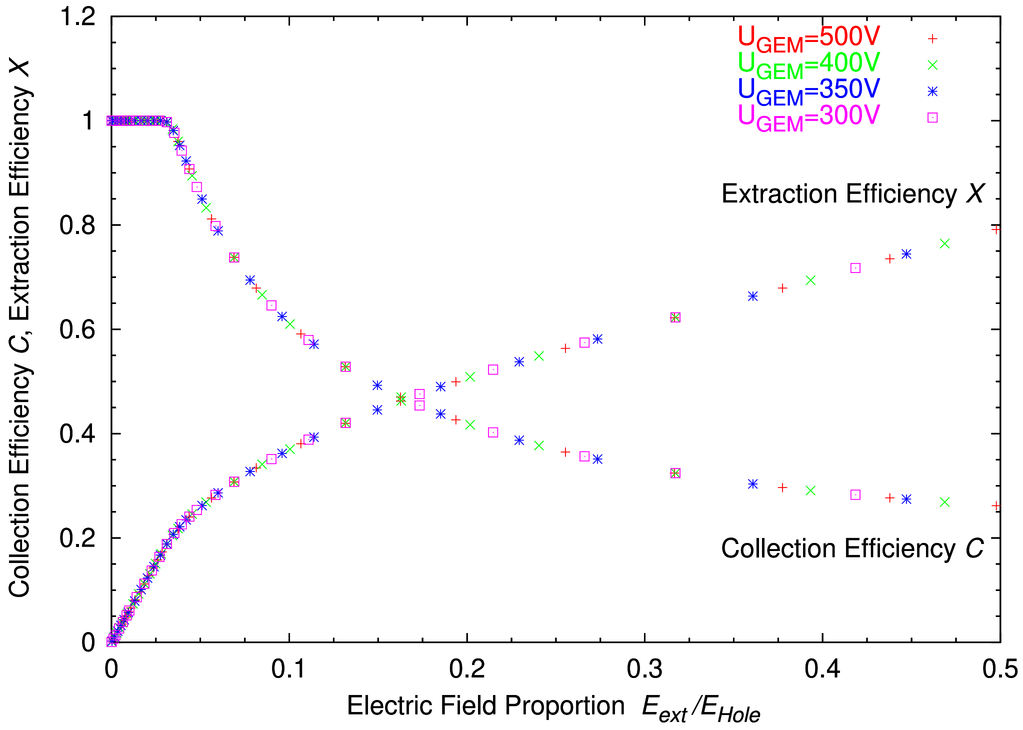

Fig. 7. Simulation of the extraction efficiency X and collection efficiency C for several GEM voltages, U_{GEM} as a function of the ratio of external and hole field

Equations 3 and 4 suggest that the collection efficiency C and extraction efficiency X both vary with the ratio between the external flux and the flux through the GEM hole. This is shown in Figure 7, where the simulation results for both coefficients are plotted versus the ratio $E_{\text{ext}}/E_{\text{hole}}$. Different markers show simulation results with different GEM voltages ranging from 300 V to 500 V.

From the field flux model also a relation between the collection and the extraction efficiency can be derived. Let Φ_{ext} be the flux onto an external electrode (anode or cathode) of size A_{ext}. As the electrode is far away from the GEM structure one can assume a homogeneous electric field and the external field strength is given by

$$E_{\text{ext}} = \frac{\Phi_{\text{ext}}}{A_{\text{ext}}} \,. \tag{5}$$

On the other hand, using the mean electric field inside the GEM hole E_{hole} as defined in Formula 1 one can write the total electric flux through the GEM hole as

$$\Phi_{\text{hole}} = E_{\text{hole}} \cdot A_{\text{hole}} \; . \tag{6}$$

Therefore, the ratio between extraction efficiency X and collection efficiency C is a linear function of the ratio between external and hole field,

$$\frac{X}{C} = \frac{\Phi_{\text{ext}}}{\Phi_{\text{hole}}} = \frac{E_{\text{ext}} \cdot A_{\text{ext}}}{E_{\text{hole}} \cdot A_{\text{hole}}} = \frac{1}{T_{\text{opt}}} \cdot \frac{E_{\text{ext}}}{E_{\text{hole}}} \; , \tag{7}$$

where the only geometrical parameter T_{opt} is the optical transparency of the GEM foil.

Figure 8 shows the predicted linear dependence between the ratio X/C and the field ratio $E_{\text{ext}}/E_{\text{hole}}$ calculated for different GEM geometries. Six different geometries describing holes with different sizes and different shapes (*conical* and *cylindrical*) have been simulated. Geometries with equal optical transparency show the same slope.

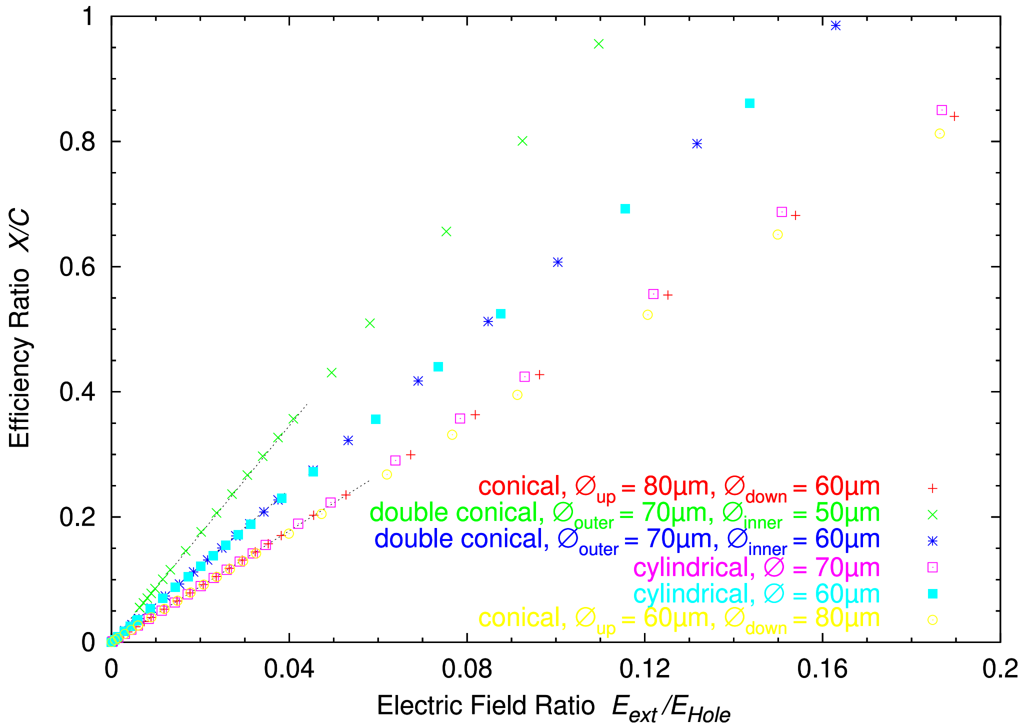

Fig. 8. The ratio X/C for different hole diameters and shapes. Conical GEM holes have an inner diameter smaller than the outer diameter at the kapton surface and cylindrical holes have a constant diameter over the total depth of the hole.

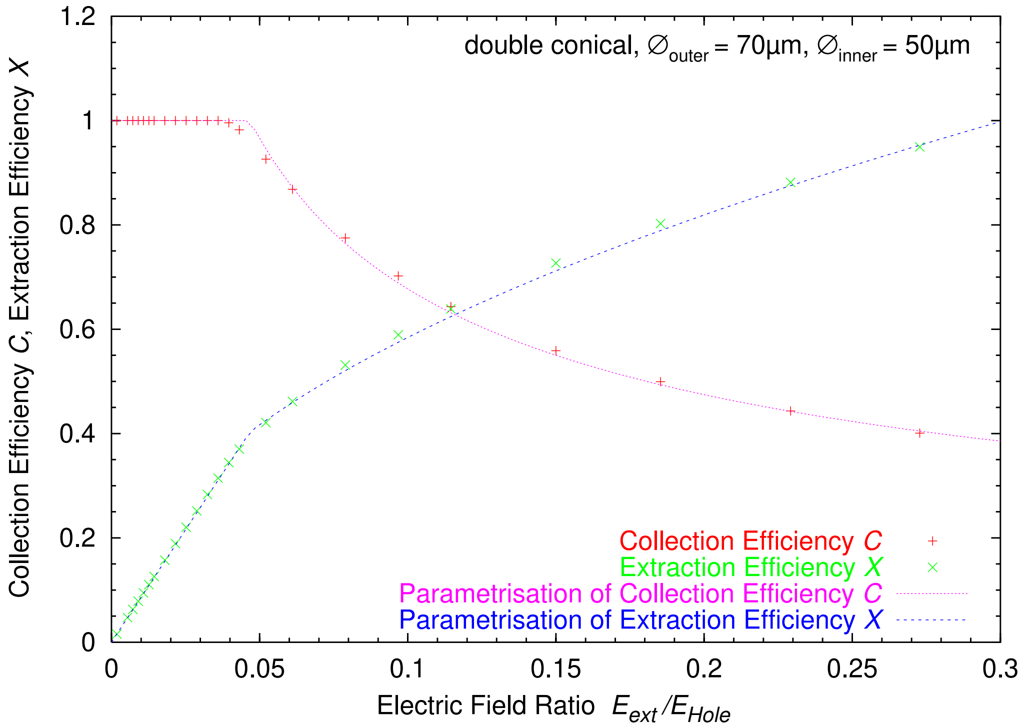

Fig. 9. Simulated efficiencies C and X compared to their parametrisations

The linear dependency between the logarithms of the collection efficiency C and the field ratio $E_{\text{ext}}/E_{\text{hole}}$ leads to a parametrisation of the simulated results using the following ansatz ($r, s \in \mathbb{R}^+$ are free parameters):

$$C = \begin{cases} 1 & \text{for} \quad E_{\text{ext}}/E_{\text{hole}} \leq r^{1/s} \\ r \cdot (E_{\text{ext}}/E_{\text{hole}})^{-s} & \text{for} \quad E_{\text{ext}}/E_{\text{hole}} > r^{1/s} \end{cases} \tag{8}$$

Following Formula 7 this gives in addition a parametrisation of the extraction efficiency X:

$$X = \begin{cases} \frac{1}{T_{\text{opt}}} \left(E_{\text{ext}}/E_{\text{hole}}\right) & \text{for} \quad E_{\text{ext}}/E_{\text{hole}} \leq r^{1/s} \\ \frac{r}{T_{\text{opt}}} \left(E_{\text{ext}}/E_{\text{hole}}\right)^{1-s} & \text{for} \quad E_{\text{ext}}/E_{\text{hole}} > r^{1/s} \end{cases} \tag{9}$$

Nearly perfect agreement between this parametrisation and the simulation results over the entire range of the field ratio can be seen from Figure 9.

4 Measurement Results and Comparison with Simulation

Figures 10 through 13 show the comparison between measurements made with the test chamber (Section 2) and the parametrisation obtained from the electrostatic simulations (Section 3).

All data except for the electron collection efficiency follow the simulation rather well. This shows that those coefficients are governed mostly by the electrostatic conditions in the chamber, not by gas effects such as diffusion. This assumption is also supported by the fact that the extraction efficiencies for electrons and ions are equal within their errors.

For the measured collection efficiency of both electrons and ions, there is a steep decrease for field ratios approaching $x = 0$ while the simulation remains constant at $C = 1$. We believe that this effect is due to recombination of charge pairs at very low drift velocities caused by the small electric field in the drift region. In contrast, while showing a plateau of $C = 1$ up to the same field ratio as the simulation, the collection efficiency for electrons decreases significantly steeper after that point. The origin of this effect is not yet understood.

The remaining difference between measurement and simulation for these variables is partly a consequence of the discrepancies between the ideal geometry of the GEM model in the simulations and the real GEMs. For example, changing the shape of the edges of the holes in the GEMs copper plating from perpendicular to the inclination of the conical holes in the polyimide causes a variation in the simulation results of the same order as the differences discussed.

The significant difference between primary and secondary ion extraction which does not occur for electrons, can be explained as follows: Through gas multiplication electrons are spread homogeneously across the cross section of every GEM hole they enter. Therefore a fraction of the electrons always occupies the radially outer regions of the hole penetrated by field lines ending on the top of the GEM and so decreasing the extraction efficiency. Primary ion extraction occurs through the same mechanism and shows the same values (compare Figures 10 and 12). However, ions subsequently collected into another GEM enter the hole in the middle, and because no multiplication and little diffusion occurs, they mostly remain on field lines continuing to the following GEM or electrode. This leads to the increased secondary extraction efficiency observed (Figure 12). Understanding these processes, calculations from electrostatic simulations describe even the effect of secondary extraction by taking into account the electric flux entering the GEM hole (Figure 6, 12).

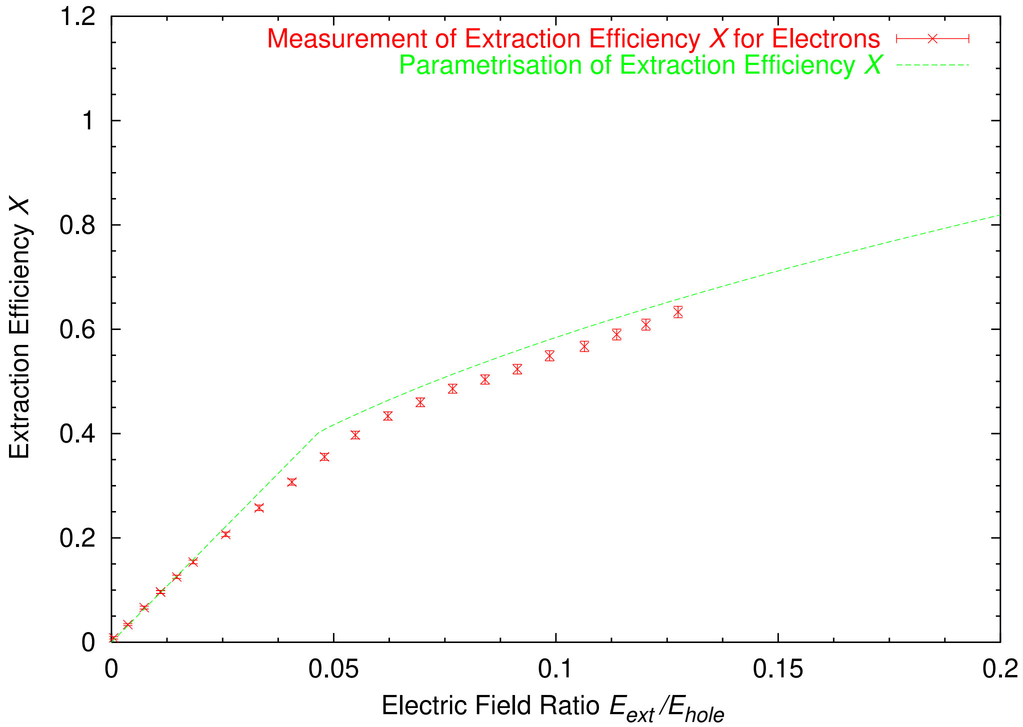

Fig. 10. Measured extraction efficiency for electrons compared to simulation.

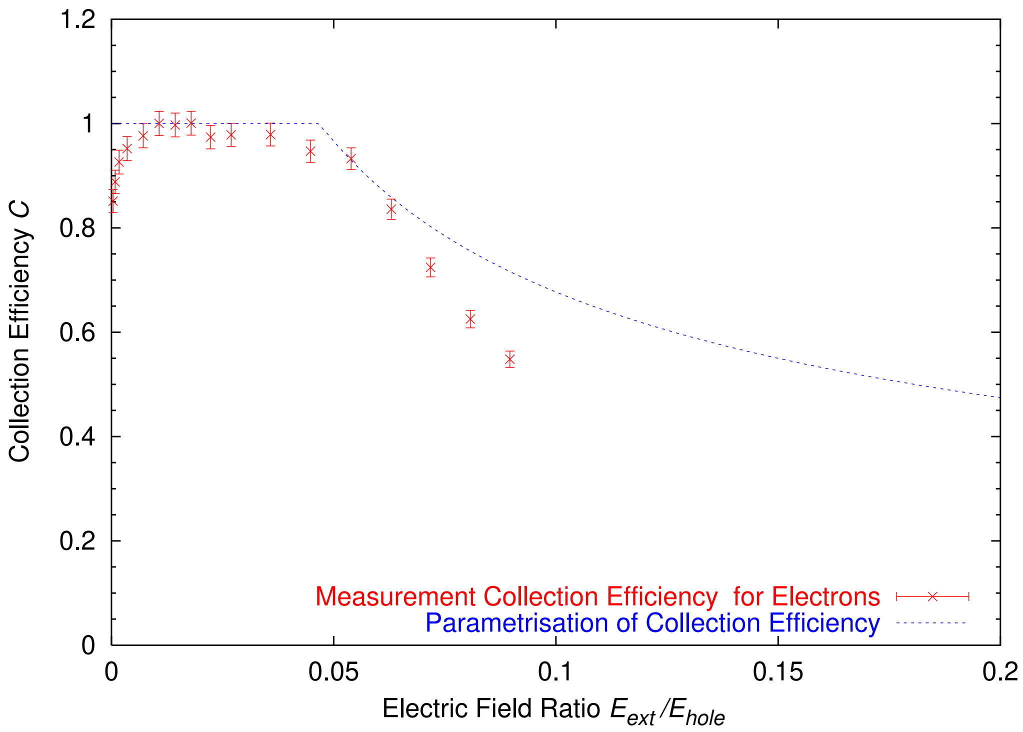

Fig. 11. Measured collection efficiency for electrons compared to simulation. As no absolute measurement was available the data points have been scaled such that collection efficiency is 100% at low field ratios as suggested by the simulation.

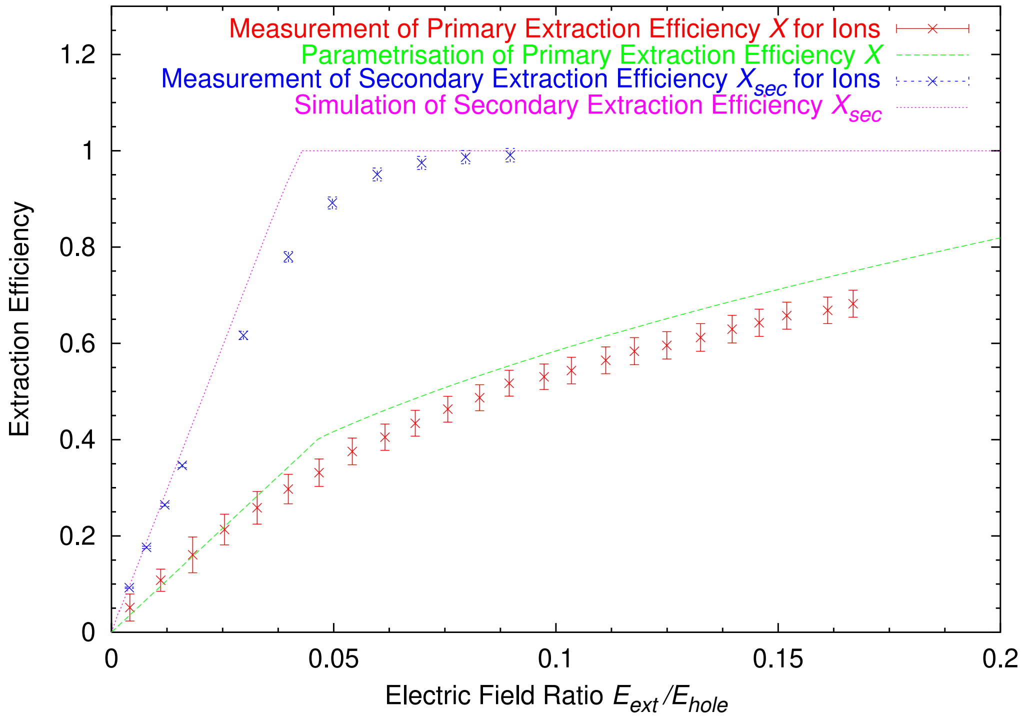

Fig. 12. Measured primary and secondary extraction efficiency for ions compared to simulation.

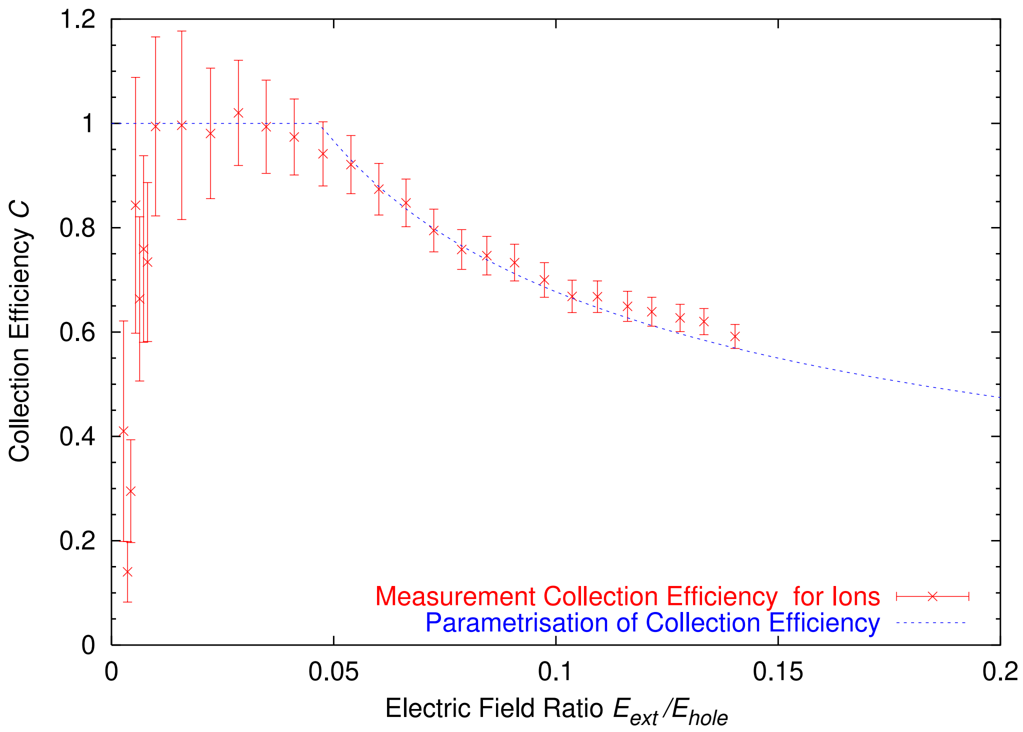

Fig. 13. Measured collection efficiency for ions compared to simulation.

5 Effect of a Magnetic Field

Our primary motivation for making tests in a magnet was to investigate whether there is a significant drop in collection efficiency for GEMs in high B-fields parallel to the electric fields as suggested by the Langevin Formula

$$\vec{v}_{Drift} \propto \hat{\vec{E}} + \omega\tau\ (\hat{\vec{E}} \times \hat{\vec{B}}) + \omega^2\tau^2\ (\hat{\vec{E}} \cdot \hat{\vec{B}})\ \hat{\vec{B}}\ , \tag{10}$$

where $\hat{\vec{E}}$ and $\hat{\vec{B}}$ are unit vectors of the fields and ω is the cyclotron frequency

$$\omega = \frac{e}{m} B\ .$$

The last term proportional to B^2, which gives the contribution along the magnetic field lines, could cause a drop in collection efficiency for high magnetic fields. When this term dominates, most electrons will no longer be collected into a GEM hole but could stay on drift lines perpendicular to the GEM surface and eventually reach the GEMs copper coating. Those charges would be lost for the signal and consequently decrease the chamber's dE/dx capabilities due to the loss in primary ionisation statistics.

5.1 Simulation

To get a first qualitative view of the electrons behaviour, we calculated drift lines in the vicinity of a GEM foil pervaded by a 4 T magnetic field. This was done using the simulation program Garfield [11] which allows consider effects of gas and magnetic fields. We use a three dimensional electric field map of a GEM at 400 V with an external field of 200 V/cm obtained with Maxwell (see Section 3). The gas mixture selected was Ar/CH_4 95/5 which is close to the mixture of $Ar/CO_2/CH_4$ 93/2/5 proposed in the TESLA Technical Design Report [1]. Each of the drift lines shown starts at a virtual straight ionisation track consisting of equally spaced electrons.

In Figure 14 the effect of the Lorentz term is well visible for electrons: they follow a track spiraling into the GEM hole. In contrast there is no contribution to the drift velocity along the magnetic field lines. Hence we have no indication for a significant drop in the collection efficiency for primary electrons.

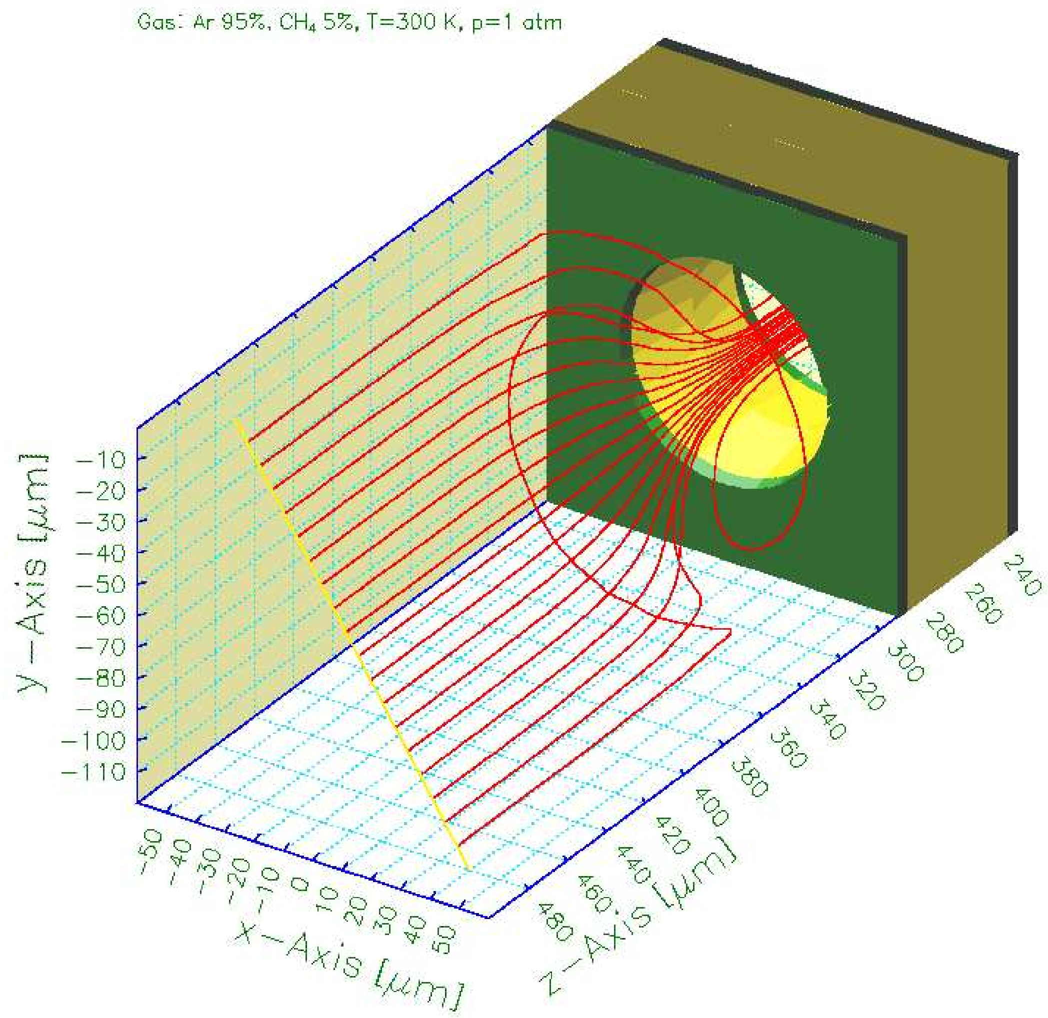

Fig. 14. Garfield simulation of drift lines in a GEM hole in a 4 T magnetic field

5.2 Measurements

For a quantitative analysis, we have conducted a series of current measurements with our test chamber in a normal-conducting magnet limited to a maximum field of 2 T. All tests were performed with a magnetic field parallel to the electric fields in the chamber.

For the test described here, we chose an electric field setup of 200 V/cm in the drift field, 5000 V/cm in the induction field and 2500 V/cm in the remaining fields. Each GEM is operated at a voltage of 310 V. The low drift field resembles the configuration in a big TPC. The gas chosen is Ar/CH_4 95/5, the same as in the Garfield simulation.

In contrast to the expected drop in collection efficiency, the signal current on the anode increases with B. At 2 T, it is approximately 6% higher than

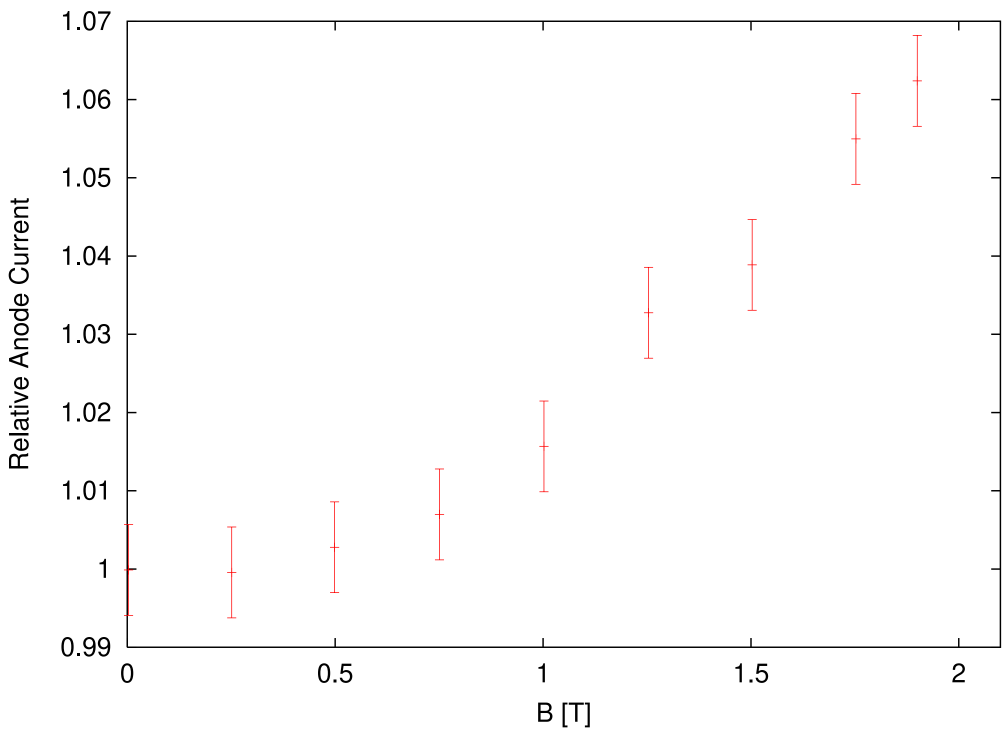

Fig. 15. Measured anode current as a function of the magnetic field

without a magnetic field. This result was at first surprising but is compatible with a decreasing collection as anticipated while being dominated by a rise in extraction efficiency or gas gain.

To investigate the mechanism for the observed rise in signal, another measurement was taken. The chamber was operated with all GEMs at 330 V and all fields at 1 kV/cm. This setting does not resemble the setting in a TPC (low drift field), but is chosen to allow simpler analysis of the charge transfer properties of the GEMs (same conditions at all GEMs, *periodic setup*): Because of the identical electrostatic conditions at all GEMs the corresponding transfer coefficients are equal and the signal current on the anode can be expressed as

$$
\begin{aligned}
I_A = I_P \cdot & C_{GEM1} \cdot G_{GEM1} \cdot X_{GEM1} \\
\cdot & C_{GEM2} \cdot G_{GEM2} \cdot X_{GEM2} \\
\cdot & C_{GEM3} \cdot G_{GEM3} \cdot X_{GEM3} \\
= \quad & I_P \cdot C^3_{GEM} \cdot G^3_{GEM} \cdot X^3_{GEM}
\end{aligned}
\qquad (11)
$$

with I_P being the current of primary ionisation by the photons from the ^{55}Fe source.

Figure 16 shows the anode current normalised to its value at $B = 0$. As before, it shows an increase with the magnetic field, this time by approximately 15%

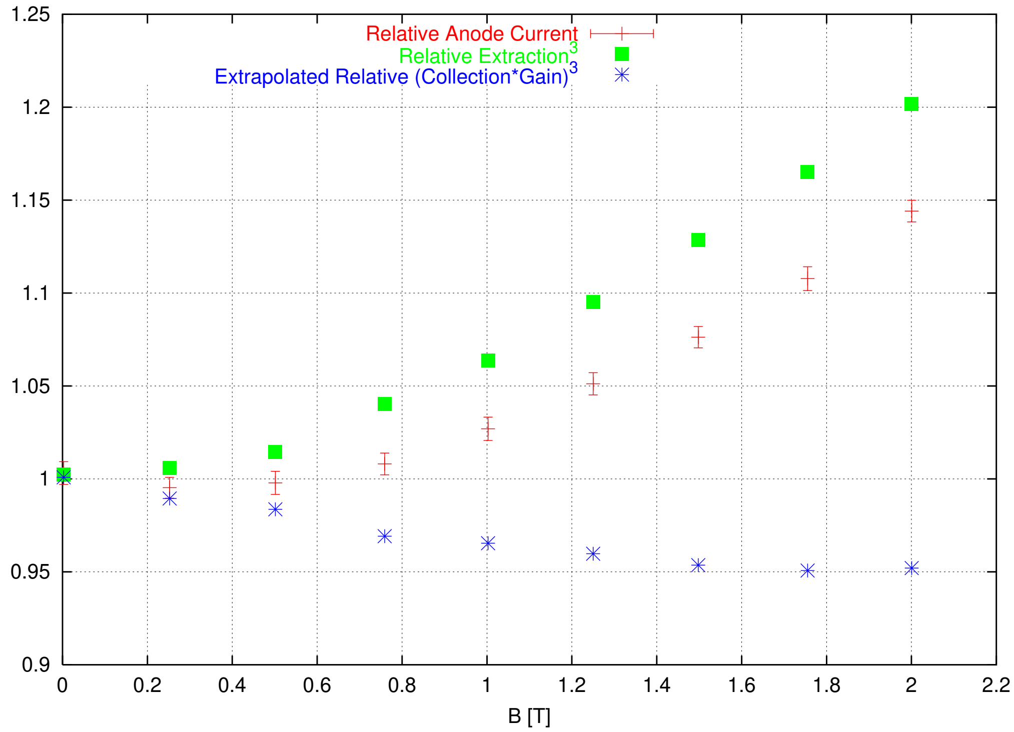

Fig. 16. Anode current vs. magnetic field for the periodic setup

at 2 T. So obviously the influence of a magnetic field on the signal current is dependent on the electrostatic chamber setup.

From the currents in the chamber recorded during the measurement the extraction efficiency of GEM3, X_{GEM3}, was calculated. As discussed above, it is the same as for the two other GEMs, $X_{GEM3} = X_{GEM}$. The squares in Figure 16 show the values of X^3_{GEM}, again normalised to their value at $B = 0$. The increase is even greater than that of the anode current (approximately 20%), which means that the product $C^3_{GEM} \cdot G^3_{GEM}$ must have decreased. Dividing the relative signal current by the calculated X^3_{GEM} yields the value of $C^3_{GEM} \cdot G^3_{GEM}$, which is plotted as stars.

Obviously, the rise in the anode current is caused by an improved extraction efficiency for high magnetic fields. A drop in collection efficiency is hardly visible (note that for a single GEM, the effect is approximately $\sqrt[3]{95\%} \approx 98\%$ which is not significant relative to the error of the measurement).

This result proves that the operation of triple GEM structures in a 2 T magnetic field is possible; for higher fields, corresponding measurements are scheduled.

6 Conclusions

It has been shown that the charge transfer coefficients of single GEM foils are predominantly determined by electrostatic conditions. Within the errors the results from measurements of the electric currents in the GEM structure are in agreement with simulations of the electric flux. The charge transfer coefficients can be described by a set of simple parametrisations which match the simulation almost identically.

A difference has been found between the extraction efficiencies of ions from the GEM holes where they were produced by gas multiplication (*primary extraction*) and from GEM holes into which the ions were collected (*secondary extraction*). Electrons do not show this behavior, because they experience multiplication (assuming a sufficiently large electric field) and are therefore distributed homogeneously across the volume of a GEM hole.

It has been demonstrated that for the working conditions in a TPC with low external field (the TPC drift field) and high electric field inside the GEM holes the ion feedback is intrinsically reduced to the percent level keeping full transparency for primary electrons. More sophisticated analysis of our parametrisation should allow the finding of an optimal field configuration of the GEM structure.

Applying a magnetic field up to 2 T perpendicular to the surface of a triple GEM structure does not result in a decrease of the effective gain. Further studies are needed to understand the quantitative behaviour of the electron collection efficiency in magnetic fields up to 4 T.

Acknowledgements

We thank F. Sauli and the CERN Gas Detector Development Group for supplying us with GEM foils and giving us a chance to look into the work of his team. We appreciate the support of T. Müller's group at University of Karlsruhe, who manufactured the test chamber parts which helped us to get a quick start in conducting measurements. We are grateful to the IKP group of Forschungszentrum Jülich, especially O. Felden and T. Sagefka, for allowing us to use their test magnet. We acknowledge the support of T. Behnke, R.D. Heuer and R. Settles and the congenial atmosphere in the Linear Collider TPC group. Finally we thank S. Bachmann fruitful discussions and the careful reading of the manuscript.

References

[1] TESLA Technical design report, Part IV, DESY-01-011, ECFA 2001-209 (2001). `http://tesla.desy.de/new_pages/TDR_CD/start.html`

[2] F. Sauli, Nucl. Instr. and Meth. A 386 (1997) 531.

[3] F. Beißel, “CUMO, HV Current Monitor, Revision V2.0”, September 1996.

[4] S. Lotze, “Aufbau eines Teststandes und Messungen zum Betrieb einer TPC mit GEMs”, diploma thesis RWTH Aachen (2001); available at `http://www.physik.rwth-aachen.de/group/IIIphys/TESLA/` .

[5] B. Sobloher, “Simulationsstudien zu GEM-Folien für die Auslese einer TPC”, diploma thesis RWTH Aachen (2002); available at `http://www.physik.rwth-aachen.de/group/IIIphys/TESLA/` .

[6] The LC TPC group, DESY-PRC R&D 01/03.

[7] F. Sauli et al., Nucl. Instr. and Meth. A 438 (1999) 376.

[8] A. Sharma, Nucl. Instr. and Meth. A 454 (2000) 267.

[9] MAXWELL, Commercial Finite Element Computation Package, Ansoft Co. Pittsburg, PA, USA.

[10] S.F. Biagi, Nucl. Instr. and Meth. A 283 (1989) 716.

[11] R. Veenhof, Nucl. Instr. and Meth. A 419 (1998) 726.